Supplement of Atmos. Chem. Phys., 20, 16117–16133, 2020
https://doi.org/10.5194/acp-20-16117-2020-supplement

Atmospheric Chemistry and Physics
Open Access

Supplement of

Soil–atmosphere exchange flux of total gaseous mercury (TGM) at subtropical and temperate forest catchments

Jun Zhou et al.

Correspondence to: Zhangwei Wang (wangzhw@rcees.ac.cn)

Supporting Text:

Site description

In the subtropical forest, the mean annual precipitation, temperature and daily relative humidity at the TFP are 1230 mm, 18.2 °C and 95%, respectively. The ecosystem type at the TFP study site is a Masson Pine dominated forest, with some associated ever-green broad-leaved species. Trees were planted in the 1960s. The soil is typically mountain yellow earth (corresponding to a Haplic Acrisol in FAO). The soil is acidic, with a pH of 3.79. From previous studies, the mean Hg concentrations in precipitation, throughfall, litterfall and organic soils were 55.3 ng L^{-1}, 98.9 ng L^{-1}, 104.8±18.6 ng g^{-1} and 191 ± 65 ng g^{-1}, respectively, with an annual Hg input of 291.2 μg m^{-2} yr^{-1} (Zhou et al., 2016;Zhou et al., 2015).

The temperate forest is located in the Xiaolongmen National Forest Park of Mt. Dongling near the Beijing Forest Ecosystem Research Station, Chinese Academy of Sciences (40°00′ N, 115°26′ E), which is located 110 km southwest of Mega-city Beijing in North China. The elevation and is 1300 m asl. The annual average rainfall is 612 mm and mean relative humidity is 66%. The Mt. Dongling is one of the Chinese Ecosystem Research Network (CERN) and Diversitas Western Pacific and Asia (DIWPA) monitoring sites. The region's climate is predominantly warm temperate continent monsoon climate with an annual average temperature 4.8 °C. Cool and dry climate in the study area has resulted in deep litter and high organic matter concentrations (Fang et al., 2007). The study area is a mature and secondary forest protected since the 1950s following the extensive deforestation. To characterize the terrestrial surface influence on the Hg fluxes, different ecosystems were selected to study the air-surface Hg fluxes from forest soil and snow at a sub-catchment (40 ha) in the temperate forest, including the Chinese pine forest, larch forest, wetland, mixed broad-leaved forest and open field. The five sites were located about 200-300 m distance individually. From previous studies, the mean litterfall Hg concentrations were 15.8, 19.6, and 12.1 ng g^{-1} in Chinese pine forest, larch forest, and mixed broad-leaved forest plots and the mean soil Hg concentrations (0-5 cm) were 72±12, 141±15, and 74±9 ng g^{-1} in Chinese pine forest, larch forest, and mixed broad-leaved forest, respectively (Zhou et al., 2017).

Environmental measurements

Daily meteorological parameters were collected and averaged over 5-min intervals. Daily air temperature and solar radiation were monitored using a TP 101 digital thermometer and a GLZ−C photo synthetically radiometer (TOP Ltd. China), respectively, during diurnal measurements. Soil percent moisture and soil temperature at 0-5 cm was monitored with Time Domain Reflectometry (TDR) Hydra Probe II (SDI−12/RS485) and a Stevens water cable tester (USA). Measurements were taken at the same time with gold trap collection. Solar radiation was collected with a weather station (Davis Wireless Vantage VUE 06250 Weather Station, Davis Instruments, Hayward, CA) located in the TFP Forest Station about 500 m away from the sub-catchment.

For each DFC sampling location, bulk soil samples were collected from the DFC footprints

(0−5 cm) in each month of study after the end of the measurement period. Soil samples were dried and homogenized, and completely ground to a fine powder in a pre-cleaned stainless-steel blender. The total Hg concentration in the soil samples was determined using a DMA-80 direct Hg analyzer (Milestone Ltd., Italy). SOM content in soils was determined using the sequential loss on ignition (LOI) method.(Zhou et al., 2013) A homogenized soil sample (WS) was dried at 105 °C for about 12- 24 h to obtain the dry weight of the samples (DW_{105}). The heated dry sample was then combusted at 550 °C for 4 h and the weight of the sample after heating at 550 °C was DW_{550}. Thus, the TOM concentration (LOI_{550}) was calculated according to the following formula:

$$LOI_{550}=100(DW_{105}- DW_{550})/WS.$$

Table S1. Characteristics and detail of measurements at five plots in the forested sub-catchments.

Forest type	Plots	Locations	Date of flux measurement				Area (%)
			Spring	Summer	Autumn	Winter	
Subtropical forest	Plot S-A	Top-slope of coniferous forest	5 Mar-7 Apr	17 -19 Jun; 1-31 Jul; 10-24 Aug	3 Nov-6 Dec	24 Dec-14 Jan	42.4
	Plot S-B	Middle-slope of the coniferous forest	5 Mar-7 Apr	17 -19 Jun; 1-31 Jul; 10-24 Aug	3 Nov-6 Dec	24 Dec-14 Jan	42.4
	Plot S-C	Wetland	5 Mar-7 Apr	1-31 Jul; 10-24 Aug	3 Nov-6 Dec	31 Dec-14 Jan	2.9
	Plot S-D	Broad-leaved forest	5 Mar-7 Apr	17 -19 Jun; 1-31 Jul; 10-24 Aug	3 Nov-6 Dec	24 Dec-14 Jan	10
	Plot S-E	Open field	22 Mar-7 Apr	17 -19 Jun; 1-31 Jul; 10-24 Aug	3-23 Nov	30 Dec-14 Jan	2.3
Temperate forest	Plot T-A	Chinese pine forest	28 Mar–25 Apr	12 Jul–10 Aug	20 Sep–20 Oct	10–16 Nov	14
	Plot T-B	Larch forest	28 Mar–25 Apr	12 Jul–10 Aug	20 Sep–20 Oct	10–16 Nov	8
	Plot T-C	Wetland	28 Mar–25 Apr	12 Jul–10 Aug	20 Sep–20 Oct	10–16 Nov	9
	Plot T-D	Mixed broad-leaved forest	28 Mar–25 Apr	12 Jul–10 Aug	20 Sep–20 Oct	10–16 Nov	65
	Plot T-E	Open field	28 Mar–25 Apr	12 Jul–10 Aug	20 Sep–20 Oct	10–16 Nov	4

Note: Area percent was according to Zhu et al. (2013) at the subtropical forest and Zhou et al. (1999) at the temperate forest.

Figure Captions:

Fig. S1. Schematic diagram of the dynamic flux chamber used in this study.

Fig. S2. Correlations between the averaged solar radiation (8:00-17:00) and air-surface Hg flux measured during daytime in Masson pine forests (a) and (b), wetland (c), evergreen broad-leaved forest (d) and open field (e) in the subtropical forest.

Fig. S3. Correlation between the averaged solar radiation (8:00-17:00) and air-surface Hg flux measured during daytime in Chinese pine forest (a), larch forest (b), wetland (c), mixed broad-leaved forest (d) and open field (e) in the temperate forest.

Fig. S4. Effects of rainfall events on annual soil-air TGM fluxes at Masson pine forests (Plot A) and (Plot B), wetland (Plot C), evergreen broad-leaved forest (Plot D) and open field (Plot E) at the subtropical forest (A), and at Chinese pine forest (Plot A), larch forest (Plot B), wetland (Plot C), mixed broad-leaved forest (Plot D) and open field (Plot E) at the temperate forest (B).

Fig. S5. Correlation between the soil Hg concentrations ($S_c \pm SD$) and soil-air Hg flux ($F \pm SD$) under the forest canopy at the subtropical forest. Standard deviations of soil Hg concentrations were obtained from Hg concentrations over the four seasons (n=12). Because fluxes are often controlled by solar radiation for bare soils, the correlation analysis above does not include data from the open field (plot E).

Fig. S6. Soil-air TGM fluxes during the daytime and nighttime at Masson pine forests (Plot A) and (Plot B), wetland (Plot C), evergreen broad-leaved forest (Plot D) and open field (Plot E) at the subtropical forest (a), and at Chinese pine forest (Plot A), larch forest (Plot B), wetland (Plot C), mixed broad-leaved forest (Plot D) and open field (Plot E) at the temperate forest (b).

Fig. S7. Correlations between soil temperature and air-surface Hg fluxes measured during daytime and night at the Masson pine forests (a) and (b), wetland (c), evergreen broad-leaved forest (d) and open field (e) in the subtropical forest.

Fig. S8. Correlations between soil temperature and air-surface Hg fluxes measured during daytime and night at the Chinese pine forest (a), larch forest (b), wetland (c), mixed broad-leaved forest (d) and open field (e) at the temperate forest.

Fig. S9. Correlations between soil moisture and air-surface Hg fluxes measured during daytime and night at the Chinese pine forest (a), larch forest (b), wetland (c), mixed broad-leaved forest (d) and open field (e) at the subtropical forest.

Fig. S10. Correlations between soil moisture and air-surface Hg fluxes measured during daytime and night at the Chinese pine forest (a), larch forest (b), wetland (c), mixed broad-leaved forest (d) and open field (e) at the temperate forest.

Fig. S11. Correlations between the gradient of Hg(0) concentrations between surface soil pore (at 3 cm) and atmospheric values and soil-air Hg(0) flux at four plots at the subtropical forest.

Fig. S12. Correlations between the gradient of Hg(0) concentrations between surface soil pore (at 3 cm) and atmospheric values and soil-air Hg(0) flux at the four plots at the temperate forest.

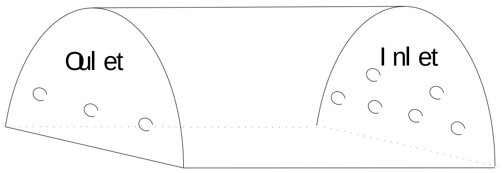

Fig. S1. Schematic diagram of the dynamic flux chamber used in this study.

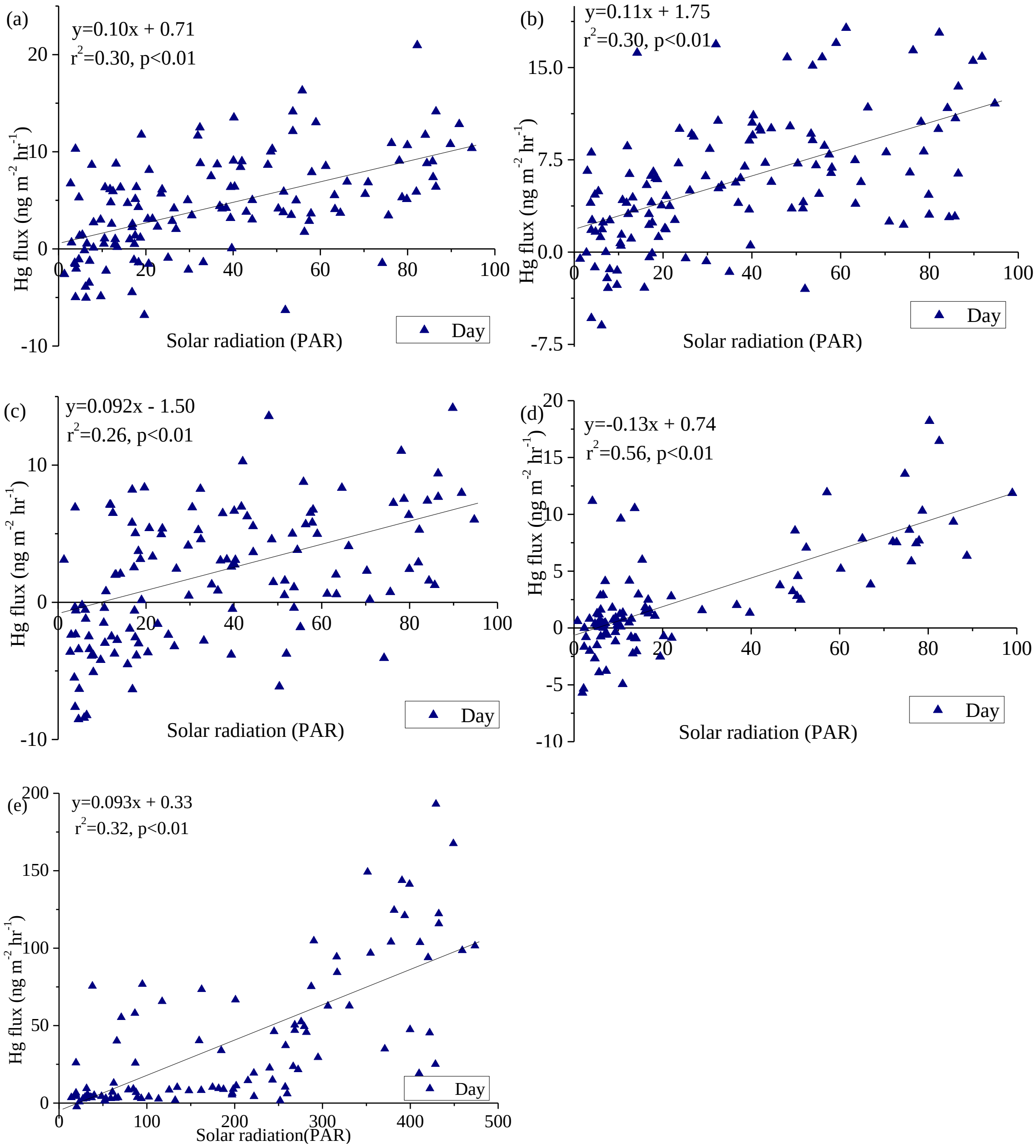

Fig. S2. Correlations between the averaged solar radiation (8:00-17:00) and air-surface Hg flux measured during daytime in Masson pine forests (a) and (b), wetland (c), evergreen broad-leaved forest (d) and open field (e) in the subtropical forest.

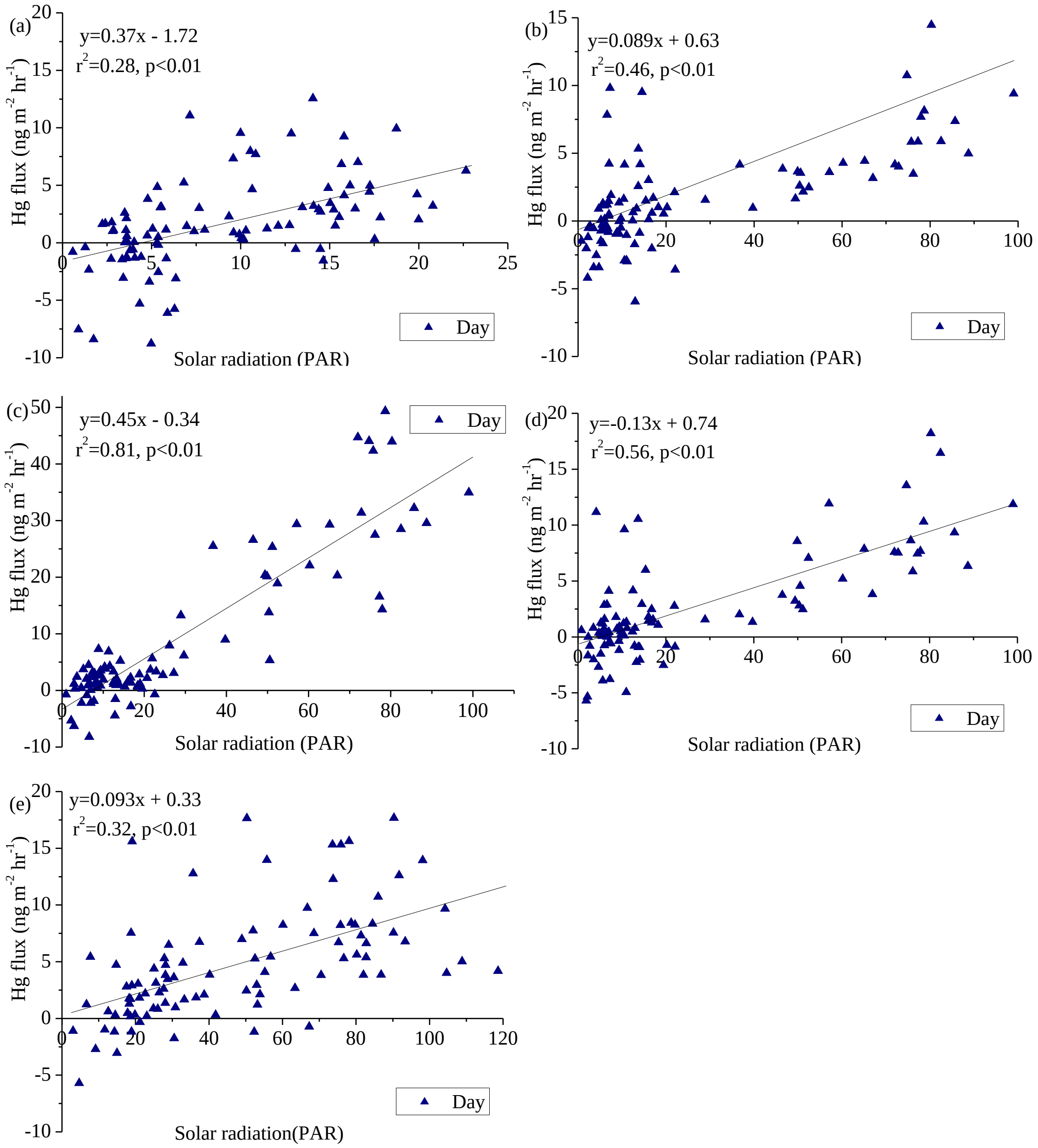

Fig. S3. Correlation between the averaged solar radiation (8:00-17:00) and air-surface Hg flux measured during daytime in Chinese pine forest (a), larch forest (b), wetland (c), mixed broad-leaved forest (d) and open field (e) in the temperate forest.

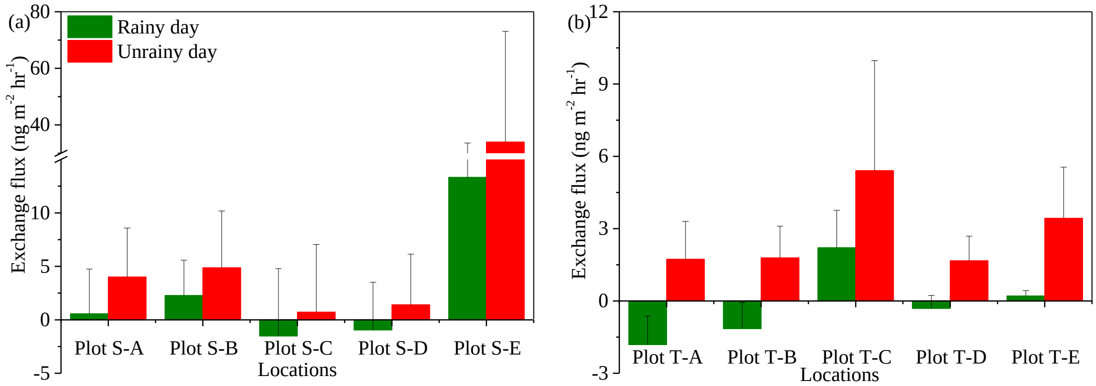

Fig. S4. Effects of rainfall events on annual soil-air TGM fluxes at Masson pine forests (Plot A) and (Plot B), wetland (Plot C), evergreen broad-leaved forest (Plot D) and open field (Plot E) at the subtropical forest (A), and at Chinese pine forest (Plot A), larch forest (Plot B), wetland (Plot C), mixed broad-leaved forest (Plot D) and open field (Plot E) at the temperate forest (B).

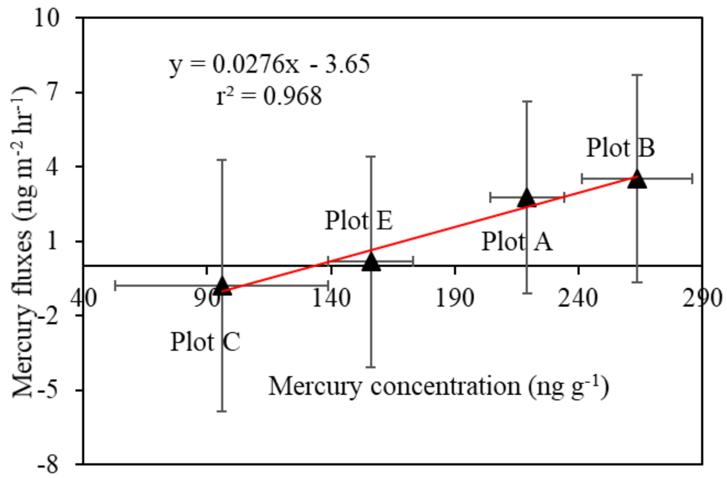

Fig. S5. Correlation between the soil Hg concentrations ($S_c \pm SD$) and soil-air Hg flux ($F \pm SD$) under the forest canopy at the subtropical forest. Standard deviations of soil Hg concentrations were obtained from Hg concentrations over the four seasons (n=12). Because fluxes are often controlled by solar radiation for bare soils, the correlation analysis above does not include data from the open field (plot E).

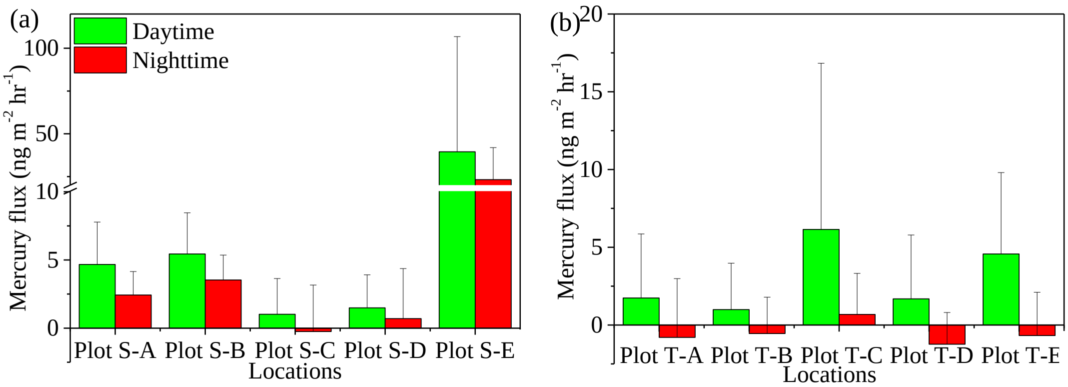

Fig. S6. Soil-air TGM fluxes during the daytime and nighttime at Masson pine forests (Plot A) and (Plot B), wetland (Plot C), evergreen broad-leaved forest (Plot D) and open field (Plot E) at the subtropical forest (a), and at Chinese pine forest (Plot A), larch forest (Plot B), wetland (Plot C), mixed broad-leaved forest (Plot D) and open field (Plot E) at the temperate forest (b).

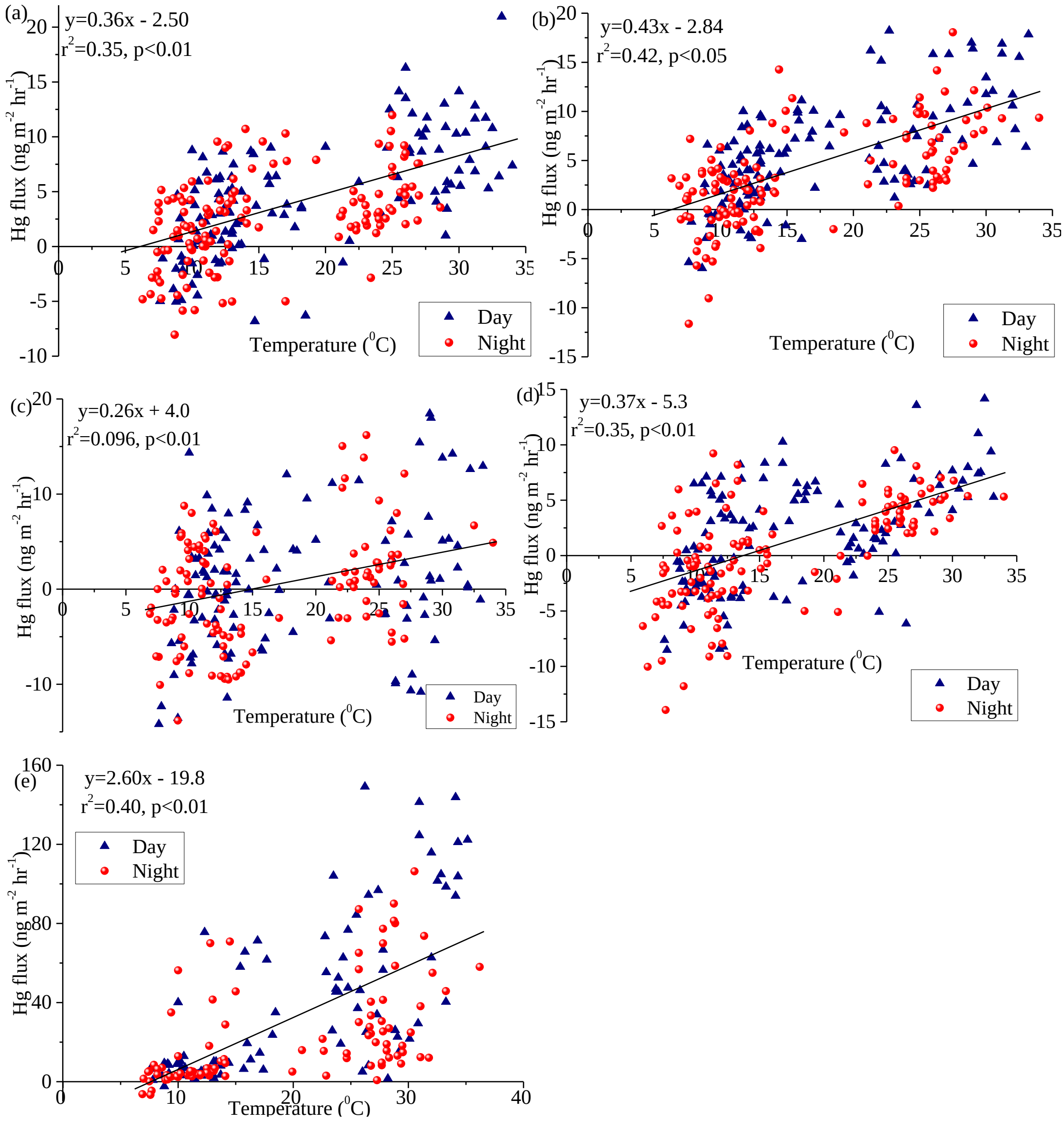

Fig. S7. Correlations between soil temperature and air-surface Hg fluxes measured during daytime and night at the Masson pine forests (a) and (b), wetland (c), evergreen broad-leaved forest (d) and open field (e) in the subtropical forest.

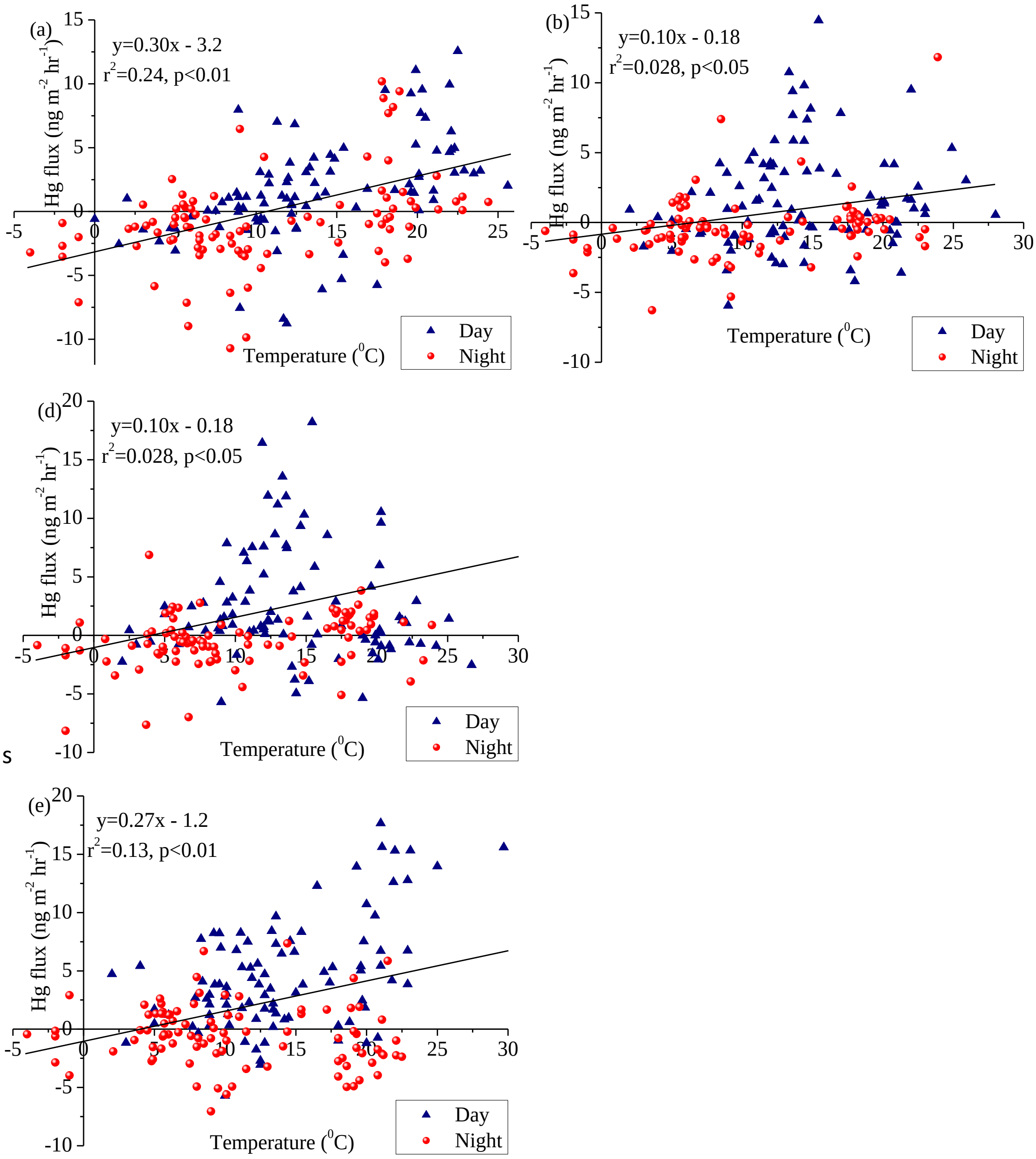

Fig. S8. Correlations between soil temperature and air-surface Hg fluxes measured during daytime and night at the Chinese pine forest (a), larch forest (b), wetland (c), mixed broad-leaved forest (d) and open field (e) at the temperate forest.

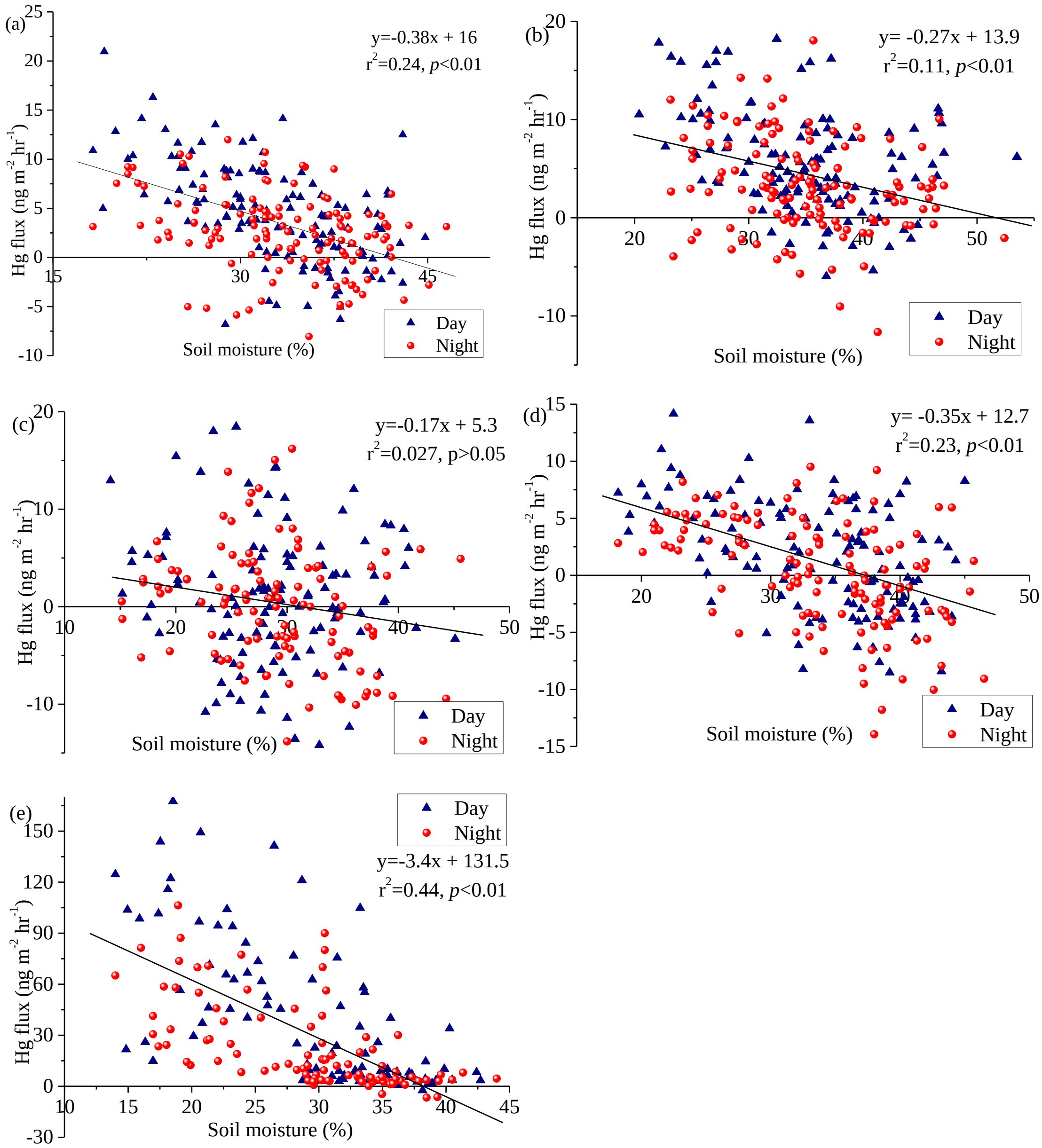

Fig. S9. Correlations between soil moisture and air-surface Hg fluxes measured during daytime and night at the Chinese pine forest (a), larch forest (b), wetland (c), mixed broad-leaved forest (d) and open field (e) at the subtropical forest.

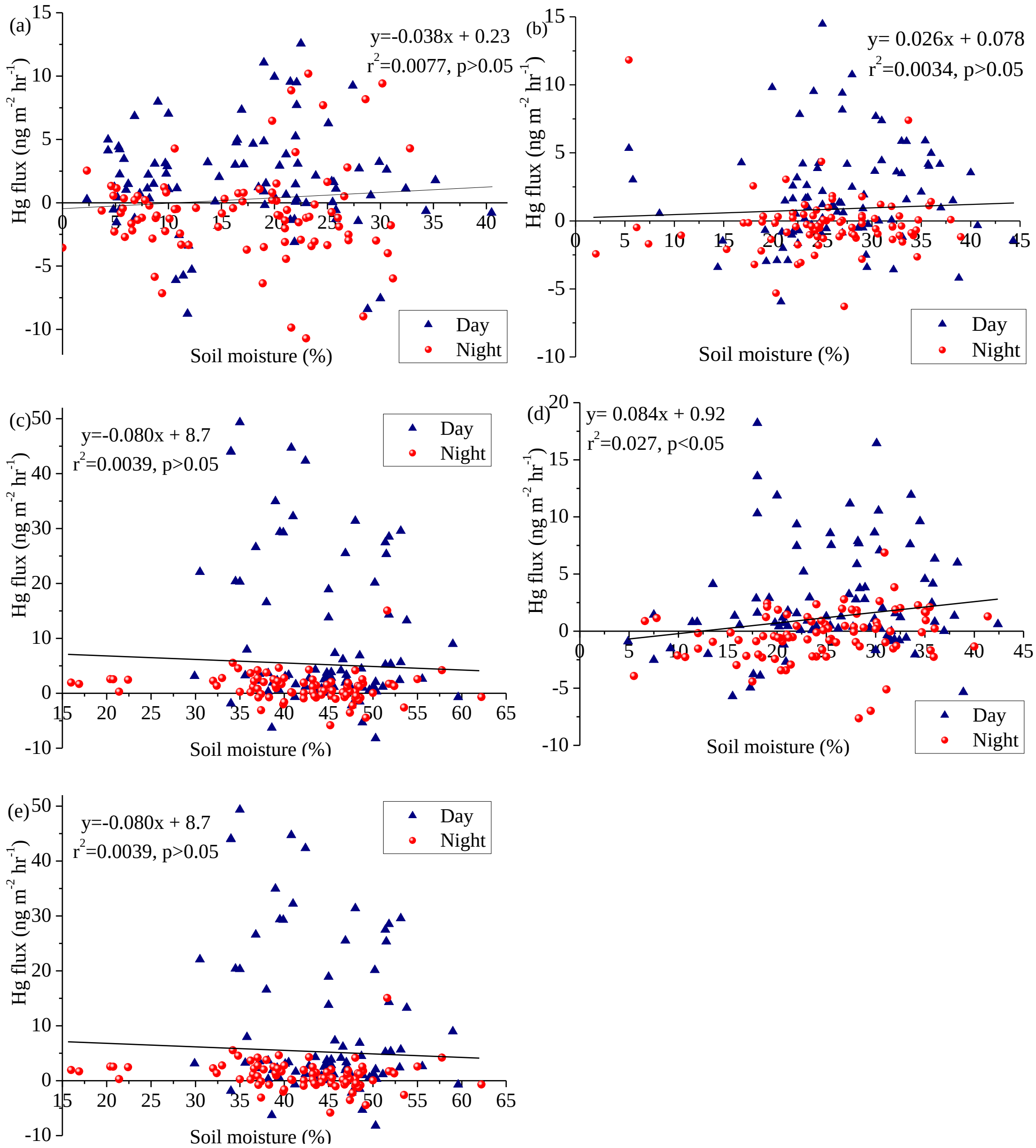

Fig. S10. Correlations between soil moisture and air-surface Hg fluxes measured during daytime and night at the Chinese pine forest (a), larch forest (b), wetland (c), mixed broad-leaved forest (d) and open field (e) at the temperate forest.

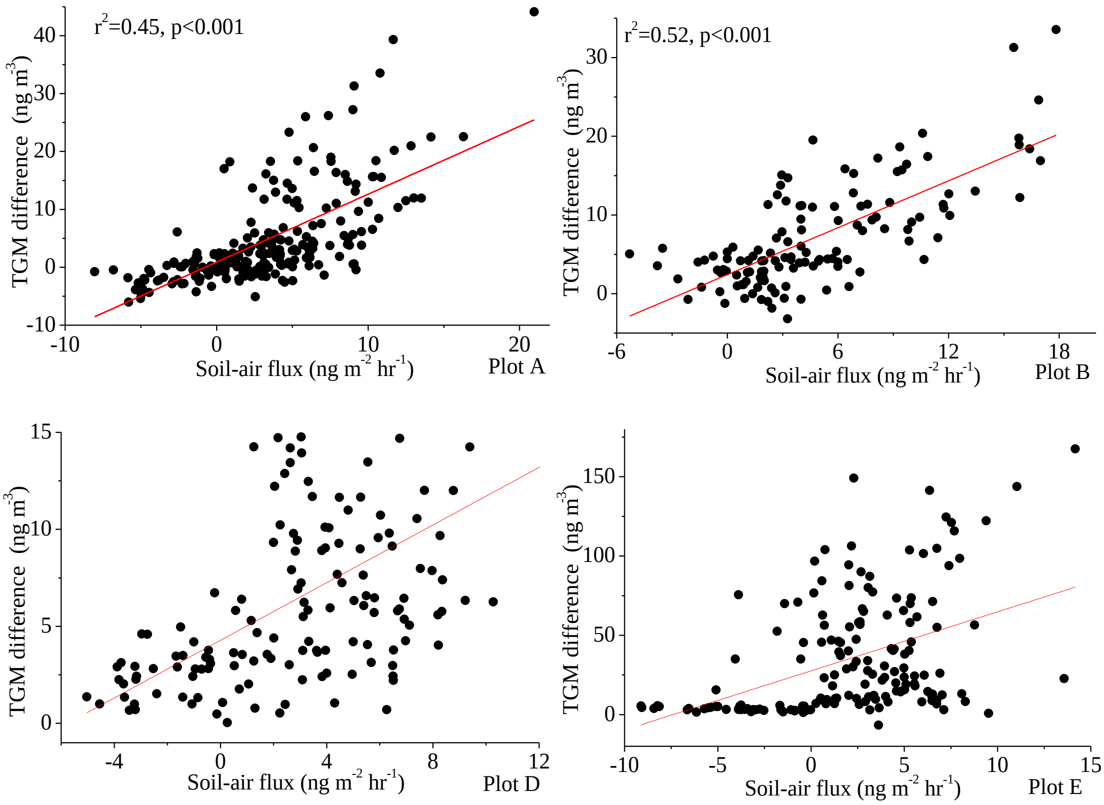

Fig. S11. Correlations between the gradient of Hg(0) concentrations between surface soil pore (at 3 cm) and atmospheric values and soil-air Hg(0) flux at four plots at the subtropical forest.

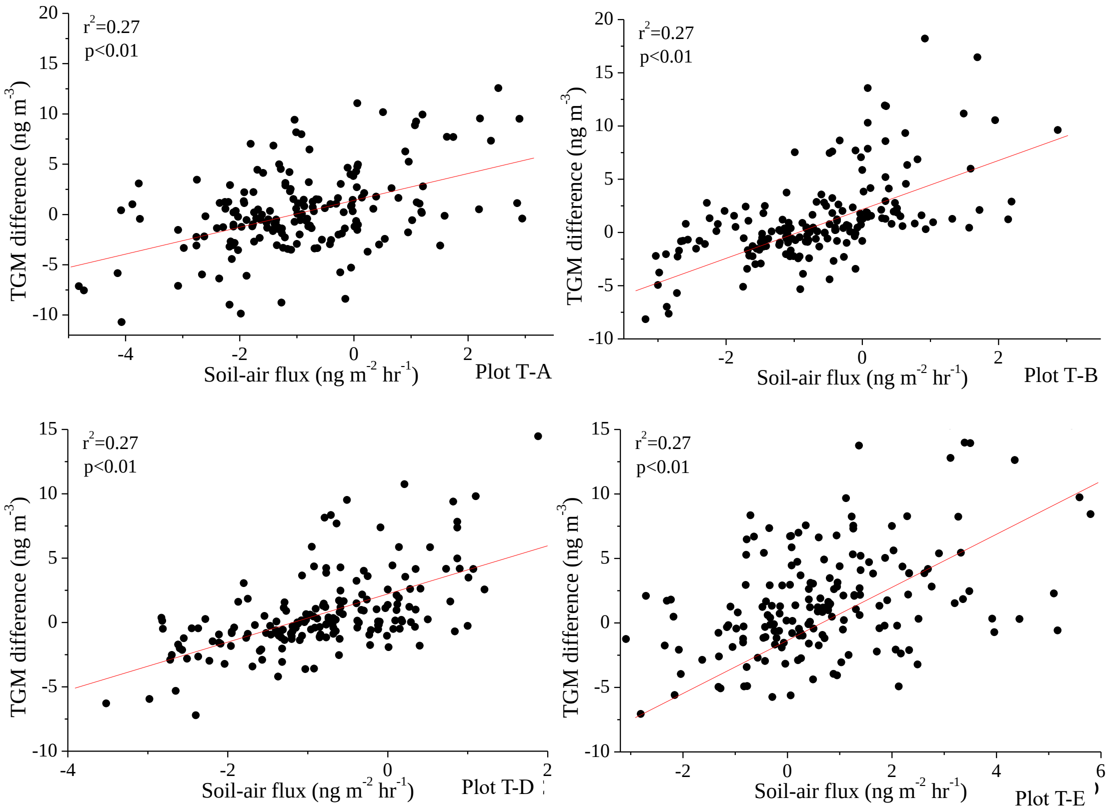

Fig. S12. Correlations between the gradient of Hg(0) concentrations between surface soil pore (at 3 cm) and atmospheric values and soil-air Hg(0) flux at the four plots at the temperate forest.

References:

Zhou, H., Ma, K., and Fu, B.: Analysis of the impacts of human activities on landscape patterns in dangling mountain area of Beijing, J Nat Resour, 14, 117-122, 1999.

Zhou, J., Feng, X., Liu, H., Zhang, H., Fu, X., Bao, Z., Wang, X., and Zhang, Y.: Examination of total mercury inputs by precipitation and litterfall in a remote upland forest of Southwestern China, Atmospheric Environment, 81, 364-372, 10.1016/j.atmosenv.2013.09.010, 2013.

Zhou, J., Wang, Z., Zhang, X., and Chen, J.: Distribution and elevated soil pools of mercury in an acidic subtropical forest of southwestern China, Environmental Pollution, 202, 187-195, 10.1016/j.envpol.2015.03.021, 2015.

Zhou, J., Wang, Z., Sun, T., Zhang, H., and Zhang, X.: Mercury in terrestrial forested systems with highly elevated mercury deposition in southwestern China: The risk to insects and potential release from wildfires, Environmental Pollution, 212, 188-196, 10.1016/j.envpol.2016.01.003, 2016.

Zhou, J., Wang, Z., Zhang, X., and Gao, Y.: Mercury concentrations and pools in four adjacent coniferous and deciduous upland forests in Beijing, China, Journal of Geophysical Research: Biogeosciences, 122, 1260-1274, 2017.

Zhu, J., Mulder, J., Solheimslid, S. O., and Dörsch, P.: Functional traits of denitrification in a subtropical forest catchment in China with high atmogenic N deposition, Soil Biology and Biochemistry, 57, 577-586, https://doi.org/10.1016/j.soilbio.2012.09.017, 2013.